Journal of
Holography and Speckle
Vol. 3, 1–8, 2006

Algorithms in Speckle-Pattern Interferometry for Recognition of Vibration Modes on Unresolved Targets

Brian G. Hoover

Advanced Optical Technologies, Albuquerque, NM, USA

Most laser measurements of complex vibrations are made either by scanning a focused probe beam over the target or by imaging the target. These measurement formats are however precluded in certain scenarios, for instance when the target is beyond the resolution limit of the optical system. In this investigation derived speckle correlations among harmonics of continuous-wave heterodyne power spectra are applied to the recognition of low-order vibration modes on an unresolved flat target. The target is represented by a set of harmonic pistons of common frequency and arbitrary complex amplitude, each of which produces a Gaussian speckle pattern. A graphical mode-recognition algorithm is based on the derived result that adjacent harmonics in power spectra due to targets with zero integrated vibration are uncorrelated. The algorithm is applicable over a range of vibration amplitudes, relative to the wavelength, dependent on the target structure, discrete, or continuous, ultimately limited by detector signal-to-noise ratio, and for continuous surfaces extendable with signal-processing steps enabled by sophisticated hardware. Sampling guidelines for continuous target surfaces are demonstrated computationally.

Keywords: Laser Vibrometry, Heterodyne Interferometry, Speckle Correlation, Mode Recognition, Micro-Doppler.

RESEARCH ARTICLE

1. INTRODUCTION

Many remote-sensing applications demand spatial characterization or assessment of a target without the spatial bandwidth required to form a conventional image. The distance at which a target becomes unresolved and appears as a point image depends on the collecting aperture of the imaging system. Celestial or orbital targets, for instance satellites, are almost always unresolved, but targets can be unresolved at any distance if the collecting aperture is sufficiently small, for instance a single-pixel detector without a lens, which might be required to minimize detector footprint, power requirements, and/or cost. Serial imaging by scanning of a focused probe spot requires transmitter bandwidth that may be unavailable for the same reasons.

Some level of spatial characterization of unresolved targets is possible through utilization of photometric, polarimetric, spectroscopic, and/or other characteristics of radiation reflected or scattered by the target,[1–3] typically along with some *a priori* knowledge of the target. Lasers provide illumination control that can facilitate such techniques, but also introduce speckle, which in most techniques is manifest as a multiplicative random variable on the detected signal.[4] Spatial characterization in the presence of speckle must therefore rely on moments or correlations among components of the detected signal, in which case characterization algorithms must be based on detailed models of the detected signal that include statistical models of speckle.[5,6] Coherent-detection techniques, for instance holographic and heterodyne electronic or digital speckle-pattern interferometry (ESPI or DSPI) provide high sensitivity and resolution, but are generally more compromised by speckle than are corresponding direct-detection techniques.[4,7]

Heterodyne ESPI/DSPI can provide spatial information about an unresolved vibrating target through the temporal variation of the interference pattern (i.e., micro-Doppler), provided that the appropriate speckle correlations are utilized. The continuous-wave (CW) heterodyne spectra of general vibration modes on an unresolved flat target are derived in Section 2.1 of this paper, with the target represented by a set of elemental harmonic pistons of common frequency and arbitrary complex amplitude, each of which produces a speckle pattern described by circular Gaussian statistics.[8] Low-order piston vibrations are represented by two elemental pistons while vibrations on continuous target surfaces are approximated by sampled sets of elemental pistons. Section 3.1 presents a graphical pattern-based algorithm for the recognition of low-order vibration

*Author to whom correspondence should be addressed.

modes based on the derived result that adjacent harmonics in power spectra due to targets with zero integrated vibration are uncorrelated. The range of vibration amplitudes over which the algorithm applies is larger for piston than for continuous-surface vibrations, but for the latter can be improved dramatically with signal-processing steps that are in the laboratory limited by hardware capabilities, which are not investigated. The applicable range is ultimately limited by detection signal-to-noise ratio.

Symbolic expressions for the spectra and spectral correlations are evaluated and plotted using Matlab 7 as described in Section 3. Reduction of the derived spectra to software allows aspects of the algorithms to be examined computationally. An example of computational analysis is given in Section 3.2, where, under limiting hardware assumptions, guidelines for sampling continuous target surfaces are demonstrated. These guidelines are relevant not only to the task of modeling vibrations on continuous surfaces, but also to performance analyses of scanning or multi-beam laser vibrometers used on arbitrary targets.[9, 10]

2. THEORY

2.1. CW Heterodyne Spectra of Unresolved Vibrations

The general model system is shown in Figure 1. The laser source is assumed to be monochromatic with frequency ω, and provides the plane wave described by $E_{\mathrm{i}}(x,\, t) = \exp[j\{k_x x - (\omega+\omega_{\mathrm{i}})t\}]$ that illuminates the vibrating target at the incident angle α, where $k_x = 2\pi \sin\alpha/\lambda_{\mathrm{i}} = (\omega + \omega_i)\sin\alpha/c$, with the frequency ω_{i} introduced by the frequency modulator (FM) in the transmitter. Initially a general one-dimensional target is assumed, the scattered field on which may be expressed as

$$E_{\mathrm{s}}(x,t)=a(x)\exp[j\{\varphi(x)+2k_z z(x,t)-(\omega+\omega_{\mathrm{i}})t\}] \quad (1)$$

where $\varphi(x)$ accounts for fixed surface scattering while $z(x,t)$ accounts for vibrations. The target is further assumed to be macroscopically flat, apart from vibratory deformations, and to have a constant reflectivity so that $a(x) = a_s \mathrm{rect}(x/L)$, with L the target length. A general harmonic vibration mode of frequency Ω is approximated by dividing the target into N segments or pistons of length L/N and writing

$$z(x,t)=\sum_{n=1}^{N} A_n \sin(\Omega t+\delta_n)\mathrm{rect}\left[\frac{N(x+\frac{L}{2N}(N-2n+1))}{L}\right] \quad (2)$$

The receiver/detector is assumed to be sufficiently far away that the target is totally unresolved, in which case the field E_D over the detector is spatially uniform, i.e., the receiver aperture is much smaller than a speckle cell.

An essential identity in the derivation of the Doppler spectrum of the target represented by Eq. (2) is the Bessel function series[11]

$$\exp(-j\mathcal{Z}\sin\theta) = \sum_{m=-\infty}^{\infty} J_m(\mathcal{Z})\exp(-jm\theta) \quad (3)$$

where $\mathcal{Z}$ is any complex number. Also, according to the Fourier shift theorem,

$$\exp(-j\mathcal{Z}\cos\theta) = \sum_{m=-\infty}^{\infty} (-j)^m J_m(\mathcal{Z})\exp(-jm\theta) \quad (4)$$

and, due to the symmetry identity $J_m(-\mathcal{Z}) = (-1)^m J_m(\mathcal{Z})$,

$$\exp(j\mathcal{Z}\sin\theta) = \sum_{m=-\infty}^{\infty} (-1)^m J_m(\mathcal{Z})\exp(-jm\theta) \quad (5)$$

2.1.1. Two Harmonic Pistons

The basic target consisting of two harmonic pistons serves to illustrate the mathematics to the point that the general heterodyne spectrum due to N pistons is obvious from the pair solution. With $N = 2$ Eq. (2) becomes

$$z(x,t) = A_1\sin(\Omega t+\delta_1)\mathrm{rect}\left[\frac{2(x+L/4)}{L}\right] + A_2\sin(\Omega t+\delta_2)\mathrm{rect}\left[\frac{2(x-L/4)}{L}\right] \quad (6)$$

and the uniform field over the detector is therefore

$$E_{\mathrm{D}}(t) = \mathscr{E}_s(0,\,t) = a_s\exp[-j(\omega+\omega_{\mathrm{i}})t] \times (\Phi_1\exp[2jk_z A_1\sin(\Omega t+\delta_1)] + \Phi_2\exp[2jk_z A_2\sin(\Omega t+\delta_2)]) \quad (7)$$

where $\mathscr{E}_{\mathrm{s}}(k,\,t)$ is the Fourier transform of the scattered field E_{s} and

$$\Phi_{1(2)} \equiv \frac{2}{L}\int_{-\frac{L}{2}(0)}^{0(\frac{L}{2})} \exp[j\varphi(x)]\,dx \quad (8)$$

are random complex constants dependent on the target surface roughness that represent the effects of speckle. Under the assumption of fully developed speckle $\Phi_{1(2)}$ are modeled as random walks with the resultant complex circular Gaussian statistics.[8]

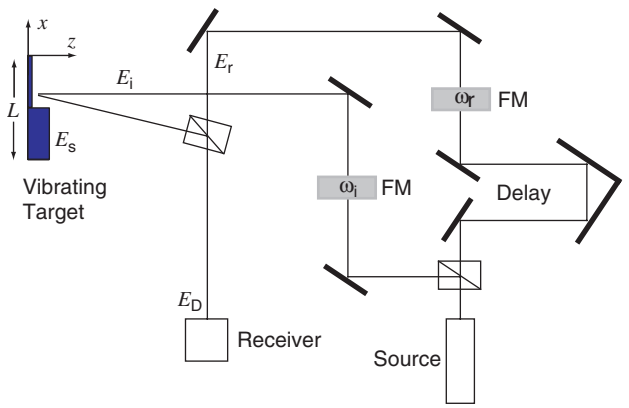

Fig. 1. Schematic of heterodyne interferometer, FM denotes frequency modulator. The scale of the target vibration amplitude in the z-direction is greatly exaggerated.

The target field of Eq. (7) interferes with the reference field $E_r = a_r \exp[-j(\omega+\omega_r)t]$ at the detector, with the recorded irradiance proportional to

$$\begin{aligned} I(t) &= \|E_D + E_r\|^2 = a_r^2 + a_s^2(\Phi_1^2 + \Phi_2^2) \\ &\quad + 2\mathrm{Re}\{a_r a_s(\Phi_1 \exp[j\{2k_z A_1 \sin(\Omega t+\delta_1)+\Delta\omega t\}] \\ &\quad + \Phi_2 \exp[j\{2k_z A_2 \sin(\Omega t+\delta_2)+\Delta\omega t\}]) \\ &\quad + a_s^2 \Phi_1 \Phi_2^* \exp[2jk_z\{A_1 \sin(\Omega t+\delta_1) \\ &\quad - A_2 \sin(\Omega t+\delta_2)\}]\} \end{aligned} \tag{9}$$

where $\Delta\omega \equiv \omega_r - \omega_i$ is the heterodyne frequency. Note that Eq. (9) assumes that the reference or local-oscillator field is completely coherent with the returned target field, although it is well-known that coherence loss compromises heterodyne detection when the round-trip distance to the target is comparable with or longer than the laser coherence length.[12]

The time-dependent or AC part of the recorded irradiance ($i(t)$) consists of the final three lines of Eq. (9). The autodyne spectrum is given for completeness in Eq. (10) but is not used in the subsequent analysis. With the phase difference between the two pistons $\delta_{12} \equiv (\delta_1 - \delta_2)/2$, the individual phases may be written as $\delta_1 = \delta_{12}$ and $\delta_2 = -\delta_{12}$. The final term of Eq. (9) is then expandable as

$$\begin{aligned} &2a_s^2 \mathrm{Re}\{\Phi_1 \Phi_2^* \exp[2jk_z\{A_1 \sin(\Omega t+\delta_{12}) \\ &\qquad - A_2 \sin(\Omega t-\delta_{12})\}]\} \\ &= 2a_s^2 \mathrm{Re}\{\Phi_1 \Phi_2^* \exp[2jk_z\{(A_1-A_2)\cos\delta_{12} \sin\Omega t \\ &\qquad + (A_1+A_2)\sin\delta_{12}\cos\Omega t\}]\} \\ &= 2a_s^2 \mathrm{Re}\{\Phi_1 \Phi_2^* \sum_{l=-\infty}^{\infty}\sum_{m=-\infty}^{\infty} (j)^m J_l[2k_z(A_2-A_1)\cos\delta_{12}] \\ &\qquad \times J_m[2k_z(A_2+A_1)\sin\delta_{12}] \exp[-j(l+m)\Omega t]\} \end{aligned} \tag{10}$$

where the final equality follows from application of Eqs. (3)–(5). Equation (10) is independent of the reference field and represents the autodyne spectrum of the oscillator pair.[3] The preceding term in Eq. (9) represents the sum of the individual heterodyne spectra of the two pistons, which, by application of Eq. (5), may be recast as

$$\begin{aligned} &2a_r a_s \mathrm{Re}\{(\Phi_1 \exp[j\{2k_z A_1 \sin(\Omega t+\delta_1)+\Delta\omega t\}] \\ &\qquad + \Phi_2 \exp[j\{2k_z A_2 \sin(\Omega t+\delta_2)+\Delta\omega t\}])\} \\ &= 2a_r a_s \mathrm{Re}\Big\{ \sum_{m=-\infty}^{\infty} (-1)^m [\Phi_1 J_m(2k_z A_1)\exp(-jm\delta_{12}) \\ &\qquad + \Phi_2 J_m(2k_z A_2)\exp(jm\delta_{12})] \\ &\qquad \times \exp[-j(m\Omega-\Delta\omega)t]\Big\} \end{aligned} \tag{11}$$

which resembles expressions in the literature for the CW heterodyne spectra of harmonic oscillators.[13] The complete Doppler spectrum is then the sum of the Fourier transforms of Eqs. (10) and (11) with the transform variable ω_D. The spectrum is symmetric about $\omega_D = 0$ since $2\mathrm{Re}\,\mathcal{Z} = \mathcal{Z} + \mathcal{Z}^*$. The overall Doppler spectrum is

$$\begin{aligned} \mathcal{J}(\omega_D) &= a_r a_s \sum_{m=-\infty}^{\infty} (-1)^m \{[\Phi_1 J_m(2k_z A_1)\exp(-jm\delta_{12}) \\ &\qquad + \Phi_2 J_m(2k_z A_2)\exp(jm\delta_{12})] \\ &\qquad \times \delta(\omega_D - \Delta\omega + m\Omega) \\ &\qquad + [\Phi_1^* J_m(2k_z A_1)\exp(jm\delta_{12}) \\ &\qquad + \Phi_2^* J_m(2k_z A_2)\exp(-jm\delta_{12})] \\ &\qquad \times \delta(\omega_D + \Delta\omega - m\Omega)\} \\ &\quad + 2a_s^2 \sum_{l=-\infty}^{\infty}\sum_{m=-\infty}^{\infty} J_l[2k_z(A_2-A_1)\cos\delta_{12}] J_m \\ &\quad \times [2k_z(A_2+A_1)\sin\delta_{12}]\delta(\omega_D + (l+m)\Omega) \\ &\quad \times \begin{cases} \mathrm{Re}\Phi_1\Phi_2^*(j)^m, & (l+m)\text{even} \\ j\mathrm{Im}\Phi_1\Phi_2^*(j)^m, & (l+m)\text{odd} \end{cases} \end{aligned} \tag{12}$$

where the first two lines represent the heterodyne spectra centered about a positive and negative heterodyne frequency, respectively, while the third and fourth lines represent the autodyne spectrum centered about $\omega_D = 0$.

Expression of the power spectrum requires assumptions on the parameters as they determine the overlap of the three terms in Eq. (12). The heterodyne frequency $\Delta\omega$ is assumed to be large enough to preclude overlap, in which case the positive heterodyne band is given by

$$\begin{aligned} \|\mathcal{J}_h(\omega_D)\|^2 &= \sum_{m=-\infty}^{\infty} \|\mathcal{J}_{hm}\|^2 \delta(\omega_D - \Delta\omega + m\Omega) \\ &= I_r I_s \sum_{m=-\infty}^{\infty} [\Phi_1^2 J_m^2(2k_z A_1) + \Phi_2^2 J_m^2(2k_z A_2) \\ &\qquad + 2J_m(2k_z A_1) J_m(2k_z A_2) \\ &\qquad \times \mathrm{Re}\{\Phi_1 \Phi_2^* \exp(-2jm\delta_{12})\}] \\ &\qquad \times \delta(\omega_D - \Delta\omega + m\Omega) \end{aligned} \tag{13}$$

A single realization of the power spectrum $\|\mathcal{J}_h(\omega_D)\|^2$ does not provide reliable estimates of the vibration parameters A_1, A_2, and δ_{12} due to the speckle parameters $\Phi_{1,2}$, which are independent, identically distributed zero-mean complex circular Gaussian random variables bounded by the unit circle. Four realizations of $\|\mathcal{J}_h(\omega_D)\|^2$ are displayed in Figure 2 for the specific case of $A_1 = A_2 = \lambda/4$ and $2\delta_{12} = \pi$, which is termed the *reciprocal* piston vibration. Speckle causes not only overall signal fluctuations, but also relative fluctuations among the spectral harmonics. Figure 2(d) illustrates so-called speckle fading or dropout that occurs when $\|\Phi_1\| \approx \|\Phi_2\| \approx 0$ and compromises most demodulation algorithms.

The speckle variation evident in Figure 2 can be partially overcome by the application of statistical moments of the spectrum. Moments can be realized in practice by

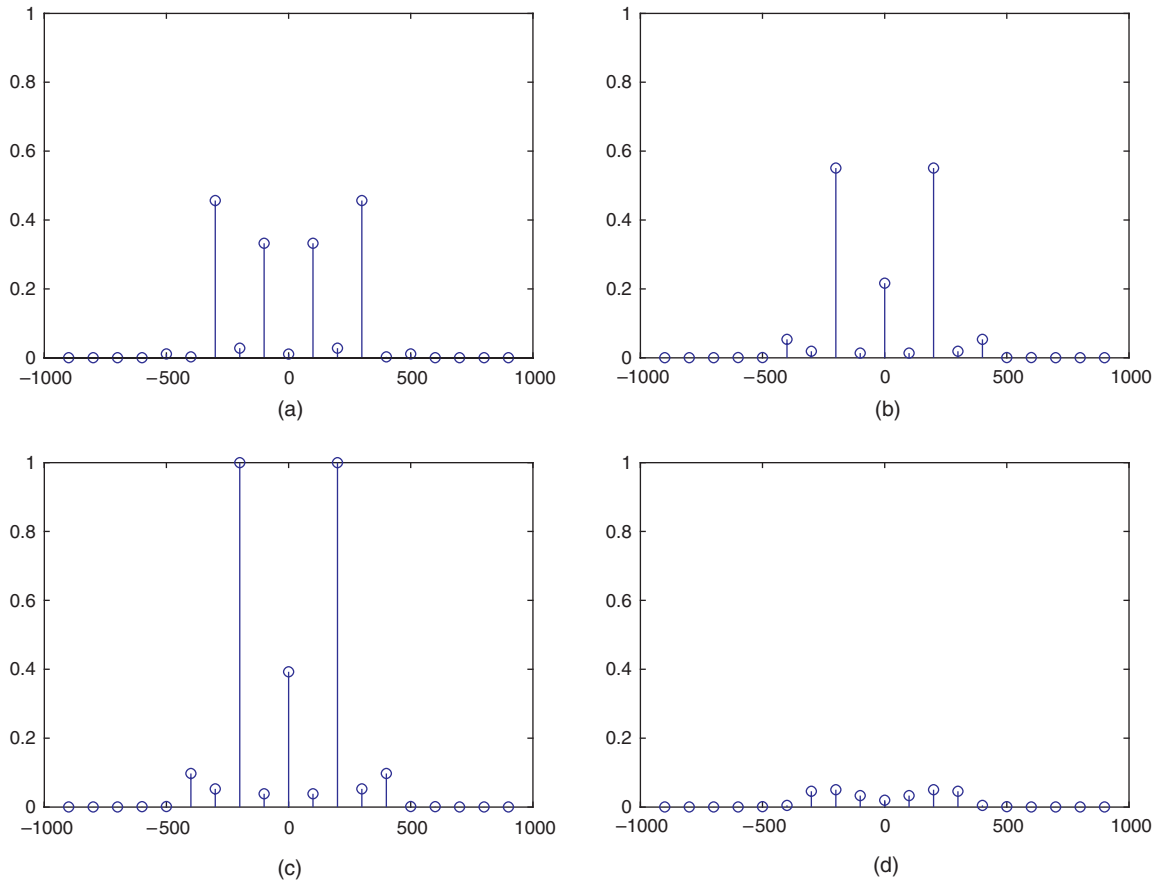

Fig. 2. Four speckle realizations of the CW-heterodyne power spectrum due to a reciprocating piston of frequency 100 Hz and amplitude $\lambda/4$. The horizontal axes are $\omega_D - \Delta\omega$. Speckle fading is exemplified in (d).

summing spectral products over ergodic measurement parameters such as the receiver angle, i.e., by moving the receiver through the speckle pattern. Target motion and beam jitter, the latter of which is unavoidable at large target distances, produce dynamic speckle patterns that can be integrated by a stationary detector, although jitter also introduces (perhaps negligible) changes in k_z. The first moment or average power spectrum depends on the vibration amplitudes A_1 and A_2 but not the phase δ_{12}. Explicitly,

$$\begin{aligned}\langle \|\mathcal{I}_h(\omega_D)\|^2\rangle &= \sum_{m=-\infty}^{\infty} \langle \|\mathcal{I}_{hm}\|^2\rangle \delta(\omega_D - \Delta\omega + m\Omega) \\ &= I_r I_s \sum_{m=-\infty}^{\infty} [\langle \Phi_1^2\rangle J_m^2(2k_z A_1) + \langle \Phi_2^2\rangle J_m^2(2k_z A_2) \\ &\qquad + 2J_m(2k_z A_1) J_m(2k_z A_2) \\ &\qquad \times \mathrm{Re}\{\langle \Phi_1 \Phi_2^*\rangle \exp(-2jm\delta_{12})\}] \\ &\quad \times \delta(\omega_D - \Delta\omega + m\Omega) \\ &= I_r \bar{I} \sum_{m=-\infty}^{\infty} [J_m^2(2k_z A_1) + J_m^2(2k_z A_2)] \\ &\quad \times \delta(\omega_D - \Delta\omega + m\Omega) \qquad (14)\end{aligned}$$

where the final equality follows from $\langle \Phi_{1,2}\rangle = 0$, and $\bar{I} = I_s\langle \Phi^2\rangle$ is the mean speckle intensity.[8] The average power spectrum of Eq. (14) is plotted in Figure 3 for the reciprocal piston vibration $A_1 = A_2 = \lambda/4$ and $2\delta_{12} = \pi$ corresponding to Figure 2. Equation (14) reveals that, due to speckle, *the average power spectrum reveals nothing about the relative phase* $2\delta_{12}$ between the piston oscillators, and is therefore insufficient for the purposes of mode recognition. In particular, the *platform* piston vibration, defined

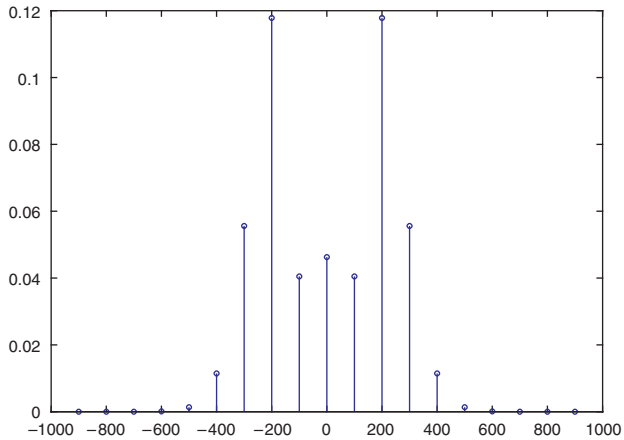

Fig. 3. Average CW-heterodyne power spectrum due to the reciprocating piston with the parameters indicated in Figure 2. The horizontal axis is $\omega_D - \Delta\omega$.

by $A_1 = A_2$ and $2\delta_{12} = 0$, has the same relative average power spectrum as the reciprocal piston vibration. These characteristics of the average power spectrum are true for any number N of elemental pistons.

On the other hand, the covariance C_{mn} between the two harmonics $\|\mathcal{J}_{hm}\|^2$ and $\|\mathcal{J}_{hn}\|^2$,

$$C_{mn} \equiv \langle \|\mathcal{J}_{hm}\|^2 \|\mathcal{J}_{hn}\|^2 \rangle - \langle \|\mathcal{J}_{hm}\|^2 \rangle \langle \|\mathcal{J}_{hn}\|^2 \rangle \quad (15)$$

$$= I_r^2 \bar{I}^2 \{ J_m^2(2k_z A_1) J_n^2(2k_z A_1) + J_m^2(2k_z A_2) J_n^2(2k_z A_2) + 2 J_m(2k_z A_1) J_m(2k_z A_2) J_n(2k_z A_1) J_n(2k_z A_2) \times \cos[2(m-n)\delta_{12}] \} \quad (16)$$

which is derived using $\langle \Phi^4 \rangle = 2\langle \Phi^2 \rangle^2$ and $\langle \mathrm{Re}\{\Phi_1 \Phi_2^*\}^2 \rangle = \langle \Phi^2 \rangle^2 / 2$,[8] depends on the relative phase between the pistons and therefore provides some capability for mode recognition. Of particular interest is the reciprocal piston vibration that corresponds to the spectra illustrated in Figures 2–3. This basic piston vibration, for which the amplitude and velocity integrate to zero over the target, produces a CW heterodyne spectrum with harmonic covariance

$$C_{mn} = 2 I_r^2 \bar{I}^2 J_m^2(2k_z A) J_n^2(2k_z A)[1 + (-1)^{m-n}] \quad (17)$$

In particular, Eq. (17) reveals that the covariance of adjacent harmonics due to this target is zero, i.e., that adjacent harmonics due to this target are uncorrelated, for any vibration amplitude A.

2.1.2. N Harmonic Pistons

The solution for the CW-heterodyne power spectrum due to a pair of diffuse piston harmonic oscillators, Eq. (13), is in a form easily extendable to the power spectrum due to multiple (N) diffuse pistons. The latter solution can be described using linear matrix algebra, which facilitates its reduction to software.

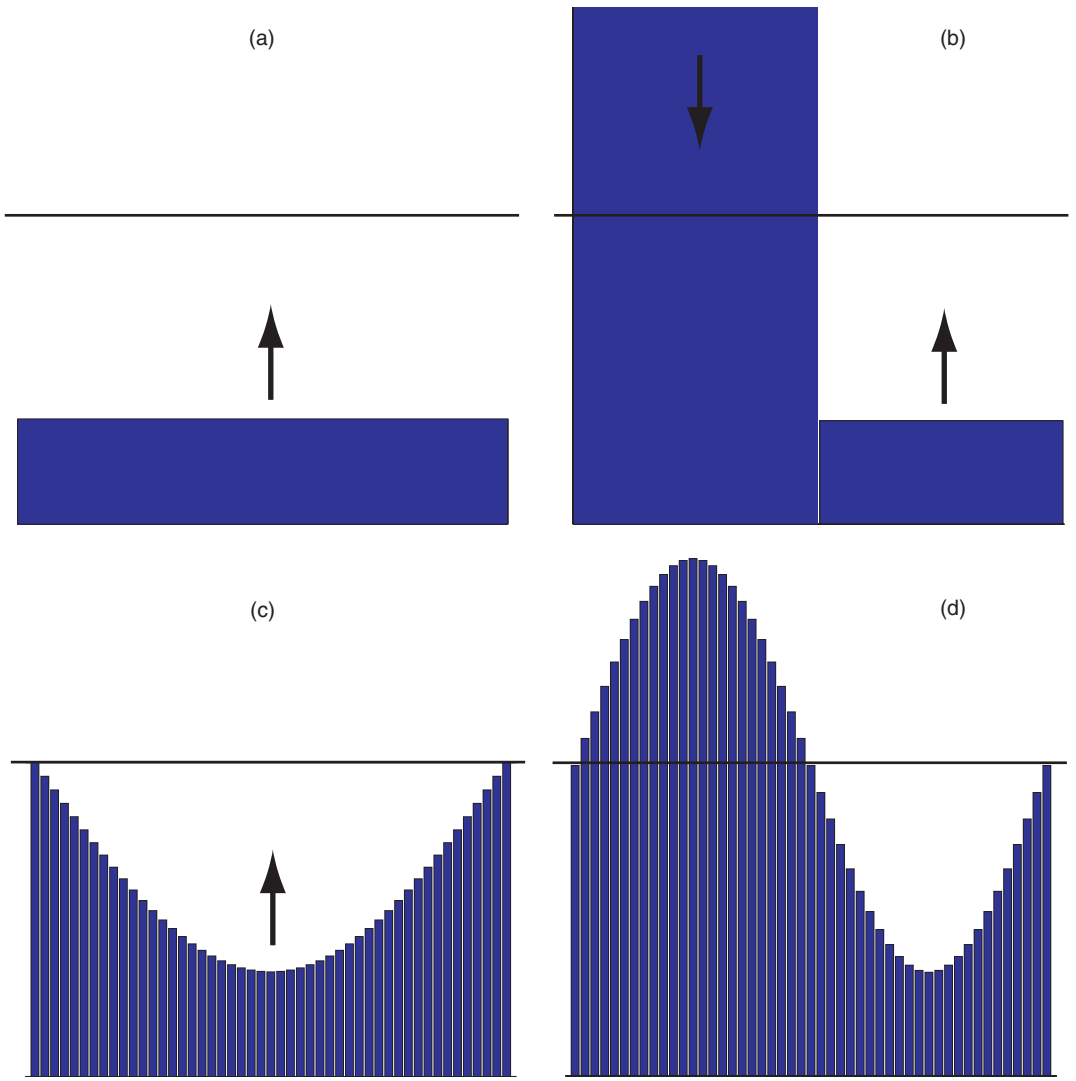

Fig. 4. Low-order vibration modes used to investigate mode-recognition algorithms: (a) Platform mode, (b) Reciprocal mode, (c) Mode 0, and (d) Mode 1. In the figure Mode 0 and Mode 1 are each approximated by 49 elemental pistons.

Let $\mathbf{PHI} = [\Phi_1\, \Phi_2 \cdots \Phi_N]$ represent the random vector of speckle amplitudes and

$$\mathbb{J} \equiv \begin{bmatrix} J_0(2k_zA_1) & J_0(2k_zA_2) & \cdots & J_0(2k_zA_N) \\ J_1(2k_zA_1) & \ddots & & \vdots \\ \vdots & & \ddots & \vdots \\ J_M(2k_zA_1) & J_M(2k_zA_2) & \cdots & J_M(2k_zA_N) \end{bmatrix} \quad (18)$$

with M the number of non-negligible harmonics in the spectrum. It can be shown that the mth harmonic is given by

$$\|\mathcal{I}_{hm}\|^2 = \frac{I_t I_s}{N^2} \sum_{i=1}^{N} \sum_{j=1}^{N} (\mathbb{J}^T \Delta_{m+1}^T \Delta_{m+1} \mathbb{J})_{ij} \times (\mathbf{PHI}^\dagger \mathbf{PHI})_{ij} \exp(j_m \mathbb{D}_{ij}) \quad (19)$$

with $\mathbb{D}_{ij} \equiv \delta_i - \delta_j$ and Δ_{m+1} the Kronecker vector with 1 in the $m+1$ column and zero elsewhere.

With the formalism of Eq. (19) power spectra can be rapidly computed for any one-dimensional vibration mode represented by an arbitrary and possibly large number of elemental pistons with arbitrary complex amplitudes. The lower limit on the size of each piston, or the upper limit on the number of pistons over a given target length L, is apparently imposed by the assumption of Gaussian speckle, which will break down when the piston area is no longer much, much larger than the coherence area of the scattered field on the piston surface.

2.2. Low-Order Vibration Modes

For the investigation of mode recognition using the preceding model results, several low-order vibration modes, which are illustrated in Figure 4, are constructed using Eq. (2) the single piston or *platform* mode, the *reciprocal* mode, and the continuous, standing-wave vibration modes referred to as Mode 0 and Mode 1. The platform and reciprocal modes are adequately represented in Eq. (2) by two elemental pistons, while Mode 0 and Mode 1 are represented by an arbitrary odd number of elemental pistons.

3. RESULTS

3.1. Graphical Recognition of Unresolved Low-Order Vibration Modes

The model results of Section 2, in particular the spectrum expressions in Eqs. (13) and (19) and the harmonic covariance of Eq. (15), can be applied to the recognition of unresolved vibration modes. This section presents a graphical algorithm, implemented through software reduction of Eqs. (19) and (15) in Matlab 7, for recognition of the low-order vibration modes illustrated in Figure 4, although the algorithm is general enough to work with a larger variety of vibration modes. Computed covariance matrices imply that the result derived in Eq. (17) for two elemental pistons, i.e., that adjacent harmonics in power spectra due to vibration modes with zero integrated vibration are uncorrelated, holds for any number of elemental pistons that constitute the reciprocal and Mode 1 vibrations over certain amplitude ranges relative to the wavelength. The recognition algorithm is based on this result. When computed covariance matrices are presented graphically, geometrical patterns associated with the various vibration modes are recognizable. Most notable is the checkerboard pattern that characterizes the covariance matrices due to modes (such as the reciprocal mode and Mode 1) with zero integrated vibration. Such a graphic computational approach lends itself to adaptation for pattern-based or visual assessment as well as extension to more general vibration modes compatible with the formalism of Section 2. The checkerboard pattern that characterizes the covariance matrix due to certain modes is very perceptible to human vision, even at low contrast, which in the current manifestation corresponds to noisy data due to incomplete speckle averaging. Obtaining covariance matrices computationally rather than analytically allows assessment of algorithm performance with incomplete speckle averages. The covariance matrices illustrated in Figures 5–7 were computed using Matlab 7 on a 1.86 GHz Intel Pentium M CPU with 1 GB RAM, on which the longest computation time (required for matrices in the bottom row of Fig. 6) was less than a minute.

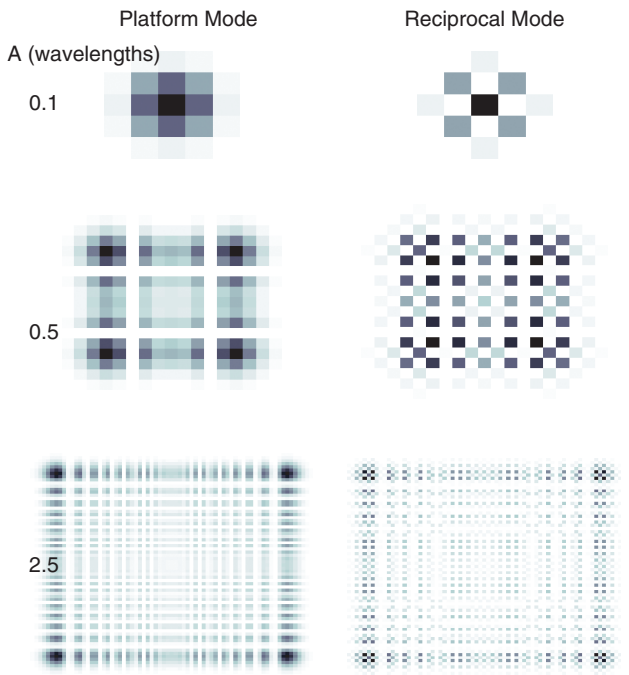

Fig. 5. Harmonic covariance matrices due to the Platform and Reciprocal modes of Figure 4 at three amplitudes each an average over 100 speckles. White represents 0 and black represents the maximum value of each matrix.

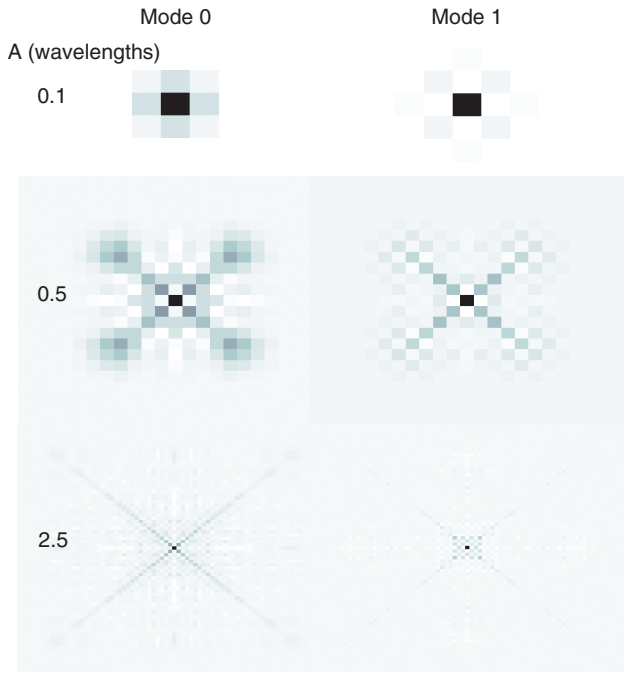

Fig. 6. Harmonic covariance matrices due to Mode 0 and Mode 1 of Figure 4 at three amplitudes, each an average over 100 speckles. White represents 0 and black represents the maximum value of each matrix.

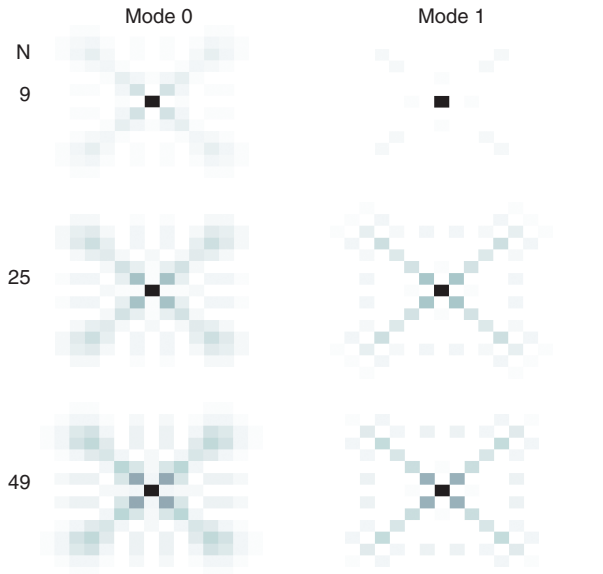

Fig. 7. Harmonic covariance matrices due to Mode 0 and Mode 1 of Figure 4 sampled at three frequencies. The vibration amplitude $A = \lambda/2$ is fixed and each matrix is an average over 5000 speckles. White represents 0 and black represents the maximum value of each matrix.

Figures 5–6 illustrate covariance matrices computed over 100 speckle patterns due to the low-order vibration modes described in Section 2.2. Figure 5 demonstrates that the checkerboard pattern predicted by Eq. (17) is strongly evident for amplitudes of the reciprocal mode over at least the range $[0.1\ 2.5]\lambda$, and that no checkerboard pattern is produced by the platform mode over at least this amplitude range. The patterns in the covariance matrices due to continuous modes shown in Figure 6 are of lower contrast than those due to piston modes shown in Figure 5, because elemental pistons with low amplitudes (near vibration nodes) contribute a bias at the fundamental heterodyne frequency $\Delta\omega$. Removal or filtering of the fundamental dramatically improves contrast and extends the range of applicability to continuous targets, but is not examined in any detail here. A low-contrast checkerboard pattern is generally obvious in the covariance matrices due to Mode 1 in Figure 6, although speckle noise is much more prominent than in the matrices due to piston targets in Figure 5. In variations caused by incomplete speckle averaging a pseudo-checkerboard pattern can also appear in the covariance matrix due to Mode 0, for instance in the low orders of the matrix of Figure 6(c), although these patterns can usually be discounted by low-order non-zero elements with $m + n$ odd, for instance C_{03} in Figure 6(c). It appears that these speckle variations can be overcome somewhat by restricting pattern recognition to higher-order elements along the matrix diagonal, although these become difficult to observe at higher vibration amplitudes without removal of the fundamental.

3.2. Sampling of Continuous Target Surfaces

This section investigates the effects of sampling on the recognition algorithm demonstrated in Section 3.1 Sampling guidelines are generally important for the reduction of analytical models to software, but, perhaps more importantly in this case, they also predict the performance of the presented algorithm based on data acquired by real scanning and multi-beam laser vibrometers, which inherently must sample target surfaces.

Basically, the graphical contrast of the checkerboard pattern that cues the mode-recognition algorithm discussed in Section 3.1 is reduced by placing any of a limited number of samples near a node of a standing-wave vibration mode. Figure 7 examines the dependence of the contrast of the harmonic covariance checkerboard pattern on the number of samples of the continuous Mode 1 at a fixed amplitude. The matrices in Figure 7 are formed as averages over 5000 speckles in order to minimize speckle effects and concentrate on sampling only. Cutting a sufficiently large number of samples in half (49 to 25) results in little loss of contrast, but the covariance matrix of 9 evenly-spaced samples, 1/3 of which are directly on vibration nodes, is effectively reduced to the fundamental, which implies that the amplitude range over which the algorithm is applicable depends on the sampling frequency. As with the matrices presented in Figure 6, this range can be extended through signal-processing steps that are not implemented here.

Acknowledgments: Thanks to Dan Senft and Victor Gamiz at the Air Force Research Laboratory, Jim Rotge and Steven Long at Boeing LTS, and Jim Roller at ATA for

technical discussions. This research was partially funded by the Air Force Research Laboratory under contract FA9451-04-C-0353.

References and Notes

1. M. Kaasalainen, K. Muinonen, and T. Laakso, *Opt. Exp.* 8, 296 **(2001)**.
2. S. Kaasalainen, J. Piironen, M. Kaasalainen, A. W. Harris, K. Muinonen, and A. Cellino, *Icarus* 161, 34 **(2003)**.
3. K. I. Schultz, D. G. Kocher, J. A. Daley, J. R. Theriault, J. Spinks, and S. Fisher, *Appl. Opt.* 33, 2349 **(1994)**.
4. P. H. Flamant, R. T. Menzies, and M. J. Kavaya, *Appl. Opt.* 23, 1412 **(1984)**.
5. S. J. Rothberg, J. R. Baker, and N. A. Halliwell, *J. Sound Vib.* 135, 516 **(1989)**.
6. A. Dabas, P. H. Flamant, and P. Salamitou, *Appl. Opt.* 33, 6524 **(1994)**.
7. K. W. Fischer and W. R. Skinner, Effect of speckle on coherent and incoherent doppler lidar, in Optical Instrumentation for Gas Emissions Monitoring and Atmospheric Measurements. *Proc. SPIE*, edited by J. Leonelli, D. K. Killinger, W. Vaughn, and M. G. Yost, **(1995)**, Vol. 2366, p. 358.
8. J. W. Goodman, Statistical properties of laser speckle patterns, in Laser Speckle and Related Phenomena, 2nd enlarged edn., edited by J. C. Dainty, Springer-Verlag, Berlin **(1984)**, Chap. 2.
9. A. K. Lal, C. F. Hess, H. Zhang, E. Hurtado, V. Aranchuk, V. B. Markov, and W. T. Mayo, Whole-field laser vibrometer for buried land mine detection, in Detection and Remediation Technologies for Mines and Mine-Like Targets VII. *Proc. SPIE*, edited by J. T. Broach, R. S. Harmon, and G. J. Dobeck **(2002)** Vol. 4742, p. 640.
10. B. J. Halkon and S. J. Rothberg, *Meas. Sci. Tech.* 14, 382 **(2003)**.
11. F. W. J. Olver, Bessel functions of integer order, in Handbook of Mathematical Functions, 9th edn., edited by M. Abramowitz and I. A. Stegun, Dover, New York **(1972)**, Chap. 9.
12. M. Harris, G. N. Pearson, J. M. Vaughan, D. Letalick, and C. Karlsson, *J. Mod. Opt.* 45, 1567 **(1998)**.
13. C. S. Vikram and T. E. McDevitt, *Opt. Eng.* 28, 922 **(1989)**.

Received: 30 June 2006. Accepted: 15 August 2006.